

Technical Note

Analysis of surface cracks in multi-crystalline thin silicon wafers



S. Saffar, B. Skallerud, Z.L. Zhang*

Department of Structural Engineering, Norwegian University of Science and Technology, NO-7491 Trondheim, Norway

ARTICLE INFO

Article history:

Received 12 July 2013

Received in revised form 11 February 2014

Accepted 15 April 2014

Available online 28 April 2014

Keywords:

Fracture mechanics

Surface crack

Silicon wafer

Stress intensity factor

Geometrical nonlinearity

ABSTRACT

Surface cracks are the most common defects in solar silicon wafers. The stress intensity factors (SIFs) calculated by the semi-analytical equation derived by Newman and Raju have been compared with results of 3D finite element analysis for a wide range of semi-elliptical surface crack configurations in thin silicon wafer subjected to bending. It has been shown that the geometrical nonlinearity of silicon wafers significantly influences the SIF values. The discrepancy between nonlinear and linear models is 19% for a surface crack with 20 μm depth and 1 mm length, while it is 74% for a surface crack with 160 μm depth and 100 mm length. Furthermore, the results show that for long surface cracks ($a/c \leq 0.01$) finite element models should be used to calculate the SIF and the existing semi-analytical solution is not reliable.

© 2014 Elsevier Ltd. All rights reserved.

1. Introduction

Surface cracks are among the most common defects in solar silicon wafers. Stress analysis of these surface-cracked wafers is needed for reliable prediction of their fracture strength. This is particularly relevant during manufacturing and transport, where the wafers are subjected to global bending. Investigators have developed approximate analytical equations, experimental methods, or engineering estimates to obtain the SIFs. Few exact solutions for three-dimensional cracked bodies are available in the literature. One of these, an elliptical crack in an infinite solid subjected to uniform tension, was derived by Irwin [1] using an exact stress analysis by Green and Sneddon [2]. Irwin also estimated the SIF for a semi-elliptical surface crack in a finite-thickness plate. His analysis is thought to be reasonably accurate for crack depths less than one-half of the plate thickness, and for small-scale yielding. Kassir and Sih [3], Shah and Kobayashi [4], and Vijayakumar and Atluri [5] obtained closed-form solutions for an elliptical crack in an infinite solid subjected to non-uniform loadings. Many authors have developed methods accounting for effects of free surfaces and plastic deformation near the crack tip on the fracture behavior of surface-cracked specimens. Some of these authors have obtained the effects of the free surfaces on stress intensity magnification factors from experimental fracture data. Hence, the magnification factors obtained are generally applicable only to the material tested. A failure criterion which is independent of crack size and specimen configuration would require detailed knowledge of the stress state near the crack tip. Smith et al. [6] and Kobayashi [7], respectively, used the alternating method to obtain SIFs along the crack front for a semi-circular surface crack in a semi-infinite solid and a semi-elliptical surface crack in a plate of finite thickness. These studies have been extended by other researchers, applying the Finite Element method (FEM) to establish more detailed knowledge of the stress state near the crack tip. Newman and

* Corresponding author. Tel.: +47 735 92530; fax: +47 735 94701.

E-mail address: zhiliang.zhang@ntnu.no (Z.L. Zhang).

Nomenclature

a	depth of surface crack, mm
b	half-length of plate, mm
c	half-length of surface crack, mm
F	stress-intensity boundary-correction factor
J_{IC}	critical J -integral, N/mm
K_I	mode I stress-intensity factor, $MPa\sqrt{m}$
K_{IC}	elastic fracture toughness
M	applied bending moment
Q	shape factor for an elliptical crack
t	plate thickness, mm
W	half-width of plate, mm
σ_b	remote bending stress, Pa
σ_m	remote uniform tension stress, Pa
φ	parametric angle of the ellipse

Raju [8,9], Nishioka and Atluri [10] used the FEM; Heliot et al. [11] used the boundary-integral equation method and the FE alternating method to determine the SIF for embedded cracks in a finite solid.

All previous studies have concentrated on regular component shapes and not on components with a very small dimension in one direction compared to the others (e.g. very thin wafers). For ease of computation, however, results expressed in the form of equations are preferable. It is important to understand the validity of these equations when applied to the thin wafers.

This paper compares the SIF calculated from semi-analytical equation and the SIF determined from J -integral obtained by 3D-finite element analysis for different size (shallow and deep) of semi-elliptical surface cracks in finite elastic wafers subjected to bending. A meshing technique is also proposed for long surface cracks in ultra-thin silicon wafers (≈ 0.2 mm thickness). This paper covers a wide range of configuration parameters. The ratio of crack depth to wafer thickness (a/t) varies from 0.025 to 0.8; the ratio of crack depth to crack length (a/c) changes from 0.001 to 0.8. The paper is organized as follows: material properties, analytical and numerical models for thin wafers are presented in Section 2 and 3. The parametric study, results and discussion are presented in Section 4. Some concluding remarks are given at the end of paper.

2. Fracture toughness and semi-analytic approach

The SIF, K_I , is a parameter which is commonly utilized in fracture mechanics to predict the stress state (“stress intensity”) near the tip of a crack caused by a remote load or residual stresses [12]. It is a theoretical construction usually applied to a homogeneous, linear elastic material and is useful to provide a failure criterion for brittle materials. The concept can also be applied to materials that exhibit small-scale yielding at a crack tip. The magnitude of K_I depends on sample geometry, the size and location of the crack, and the magnitude and the modal distribution of loads. The SIF for a semi-elliptical surface crack in a flat plate can be expressed [8,9]:

$$K_I = (\sigma_m + H\sigma_b) \sqrt{\frac{\pi a}{Q}} F\left(\frac{a}{t}, \frac{a}{c}, \frac{c}{W}, \varphi\right) \quad (1)$$

for $0 < a/c \leq 1$, $0 \leq a/t < 1$, and $c/W < 0.5$. Here H , Q and F are the boundary- correction factors.

A crack begins to propagate when the SIF reaches a critical value. The critical value is a material dependent parameter and is called fracture toughness (K_{IC}). The $K_{IC} = 0.75 \pm 0.06 \text{ MPa} \times \sqrt{m}$ is employed as fracture toughness for multi-crystalline silicon material in this study [13]. Numerically, SIFs were obtained via the J -integral calculated from FEM, using $J = K_I^2/E^*$, where E^* is the elastic modulus in plane strain condition.

3. Model geometry, load and boundary condition

The dimensions of the silicon wafers modeled in the present study are $156 \times 156 \times 0.2 \text{ mm}^3$. A 3D finite element analysis was used to calculate the J -integral variations along the crack front for a surface crack in a thin silicon wafer. The wafer was subjected to a bending load shown in Fig. 1. The nominal outer-layer bending stress is calculated from the applied bending moment M . The mode I SIF, K_I , is calculated for any point along the surface crack front by both the semi-analytical equation and finite element analysis. The bending stress which is used to calculate K_I from semi-analytical equation is the same as the one obtained from FEM considering geometrical nonlinearity. Due to symmetry of the wafer geometry, boundary and load conditions, only one quarter of the overall model is built to minimize computational time. The external load is applied as a moment, and the J -integral is extracted from the simulations in each load increment. Two types of finite element meshing are used in this study. Semi elliptical shape is used for $a/c \geq 0.25$ which is denoted as model A. A combination of a quarter

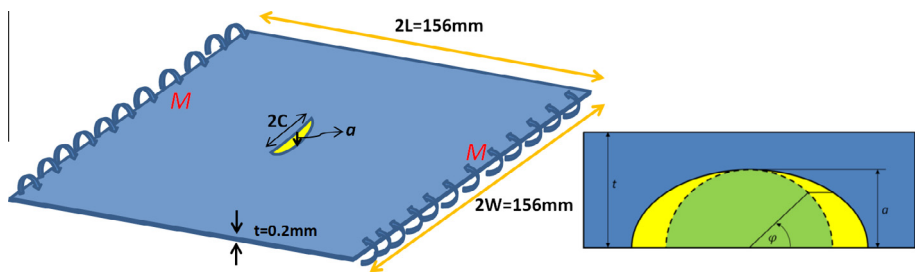


Fig. 1. Crack parameters, boundary and loading condition.



Fig. 2. Built model from the realistic multi-crystal silicon wafer.

Table 1
Crack geometry.

Crack depth a (mm)	Half crack length c (mm)
0.005	0.00625 to 50
0.01	0.0125 to 75
0.02	0.025 to 75
0.04	0.05 to 75
0.08	0.1 to 75
0.16	0.2 to 75

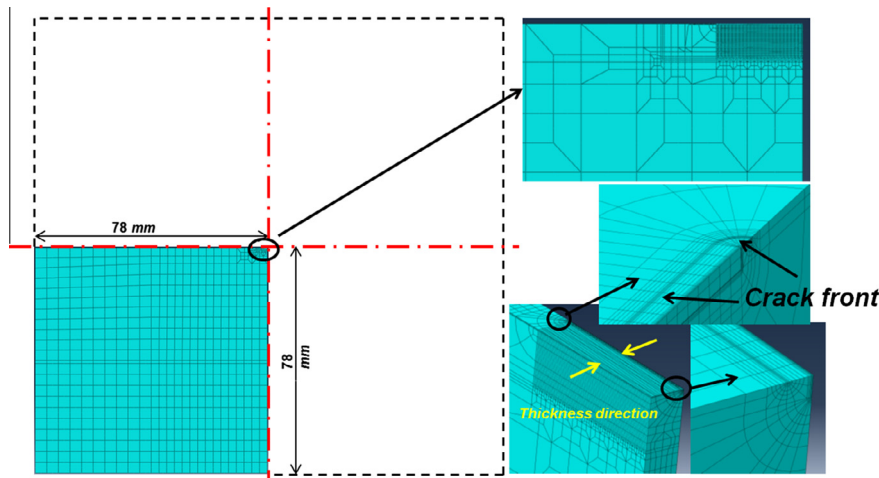


Fig. 3. Sample of mesh used in crack area.

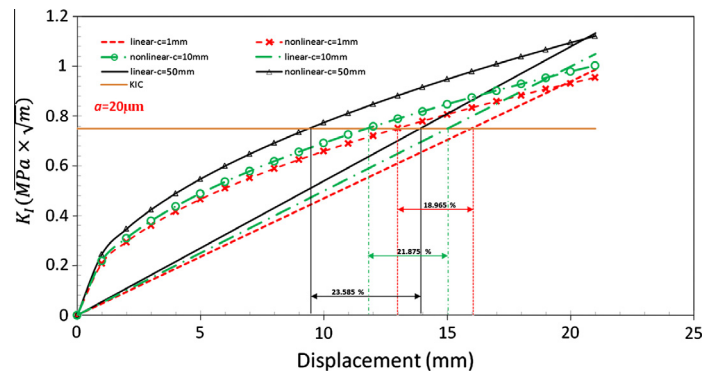


Fig. 4. Comparison of the SIF between linear and nonlinear models for crack with 20 μm depth.

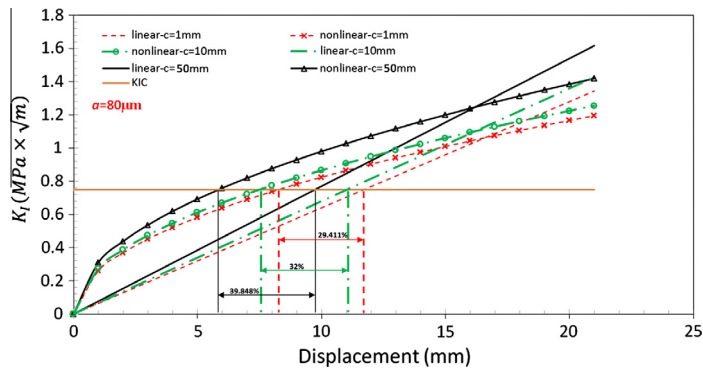


Fig. 5. Comparison of the SIF between linear and nonlinear models for crack with 80 μm depth.

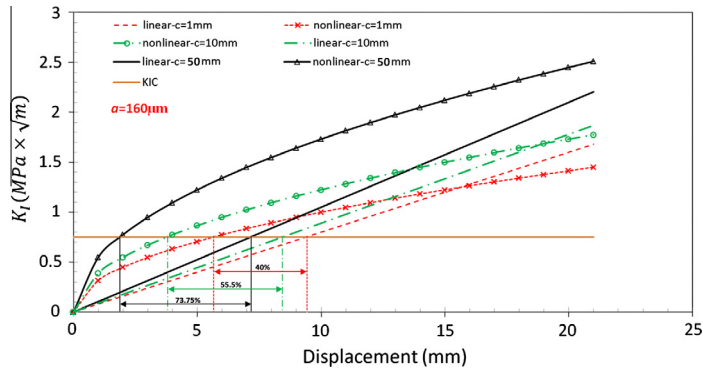


Fig. 6. Comparison of the SIF between linear and nonlinear models for crack with 160 μm depth.

circle at each end connected by a straight line is employed for long cracks ($a/c < 0.25$) which is denoted as model B in the rest of the paper. Fig. 2 shows an example of model B for a crack of depth 20 μm and length 1 mm. Since thin wafers are flexible and can develop large deflections under transverse loadings, the geometric nonlinearities during the deformation process are included in the FEA simulations as large displacement analysis is carried out. Preliminary analysis showed that the differences in the results obtained from linear and nonlinear simulations are sufficiently large to indicate that a linear simulation is not adequate for these wafers. Similar conclusion in this regard was also drawn in Ref. [13]. Briefly, the model assumptions are:

- Crack plane is perpendicular to the wafer surface.
- The entire wafer fractures once crack starts to propagate.

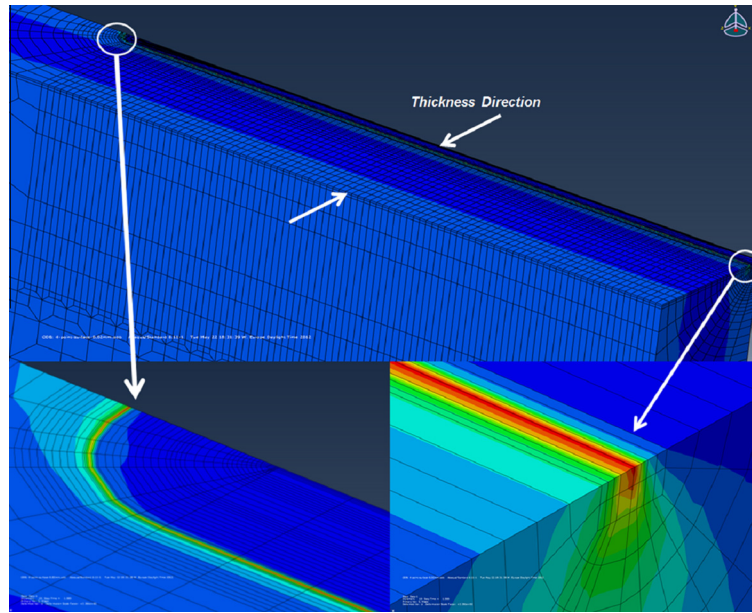


Fig. 7. Typical stress distribution in crack tip for a crack with 1 mm length and 20 μm depth.

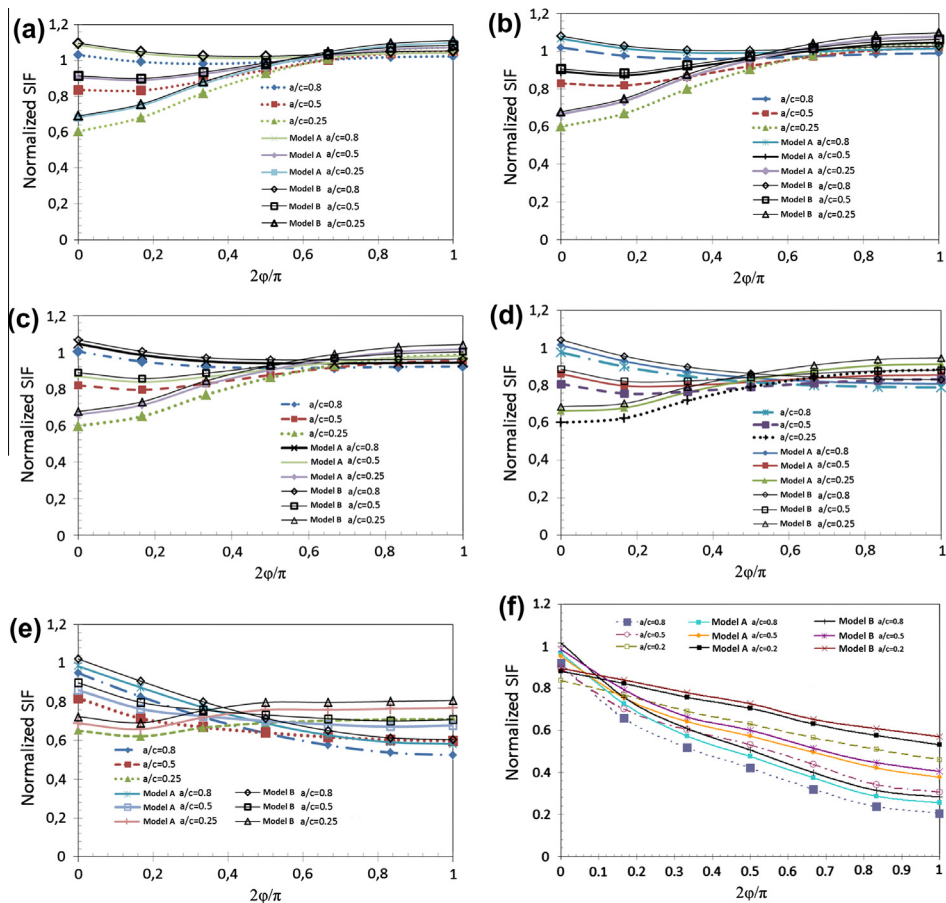


Fig. 8. Comparison of Normalized SIF between the FEM solutions and existing equations for cracks with depths (a) 0.005 mm, (b) 0.01 mm, (c) 0.02 mm (d) 0.04 mm (e) 0.08 mm (f) 0.16 mm for range of $0.25 \leq a/c \leq 0.8$.

- The whole system is linear elastic.
- Although silicon is an anisotropic material [14–16], it is considered as an isotropic material in the present study.

Regarding the final bullet point, the anisotropy may lead to variations in SIF components compared to the isotropic case. However, the main focus of the present study is the effect of crack size and shape, and the same material simplification is employed for the semi-analytical and numerical approach. The issue of anisotropy should be addressed in future studies. The values of Young's modulus and Poisson ratio for cast multi-crystalline silicon reported in the literature are taken as $E = 162.5$ GPa and $\nu = 0.223$, respectively [13].

Furthermore, to show that multi-crystalline and isotropic silicon wafers do not show significant differences in magnitude of stress, the multi-crystalline silicon wafer is modeled with different material orientations to investigate the effect of crystalline on static loading.

As mentioned before, multi-crystalline silicon wafers are anisotropic in nature. Anisotropic material properties are specified using the stiffness matrix defined in the proper coordinate system (x, y, z) [17]. The stiffness coefficients are obtained from the known compliance coefficients for single crystal silicon with respect to the crystal coordinate system. In general, multi-crystalline silicon wafers are characterized by a $\{110\}$ surface and a $\langle 112 \rangle$ growth direction [18]. Therefore, the stiffness is specified using the $\{110\}$ single-crystal properties with $[11-2]$, $[1-11]$ and $[110]$ orientations representing the x, y and z axes, respectively. The resulting elastic stiffness matrix (in GPa) for the silicon wafer is given

$$C_{ijkl}^{Cz} = \begin{bmatrix} 165.64 & 63.94 & 63.94 & 0 & 0 & 0 \\ & 165.64 & 63.94 & 0 & 0 & 0 \\ & & 165.64 & 0 & 0 & 0 \\ & & & 79.51 & 0 & 0 \\ & & & & 79.51 & 0 \\ \text{sym} & & & & & 79.51 \end{bmatrix} \quad (2)$$

In the analysis of multi-crystalline silicon wafers this stiffness matrix will be rotated for each grain independently. The values of density and Poisson ratio are kept the same as the isotropic case.

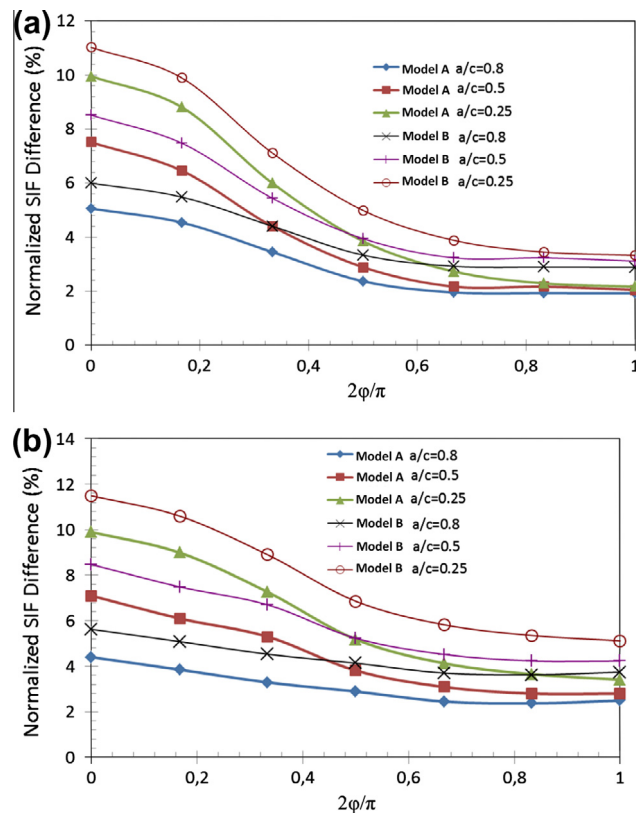


Fig. 9. Comparison of normalized SIF differences between Newman-Raju equation and FEM for crack with depth (a) 0.005 mm, (b) 0.01 mm.

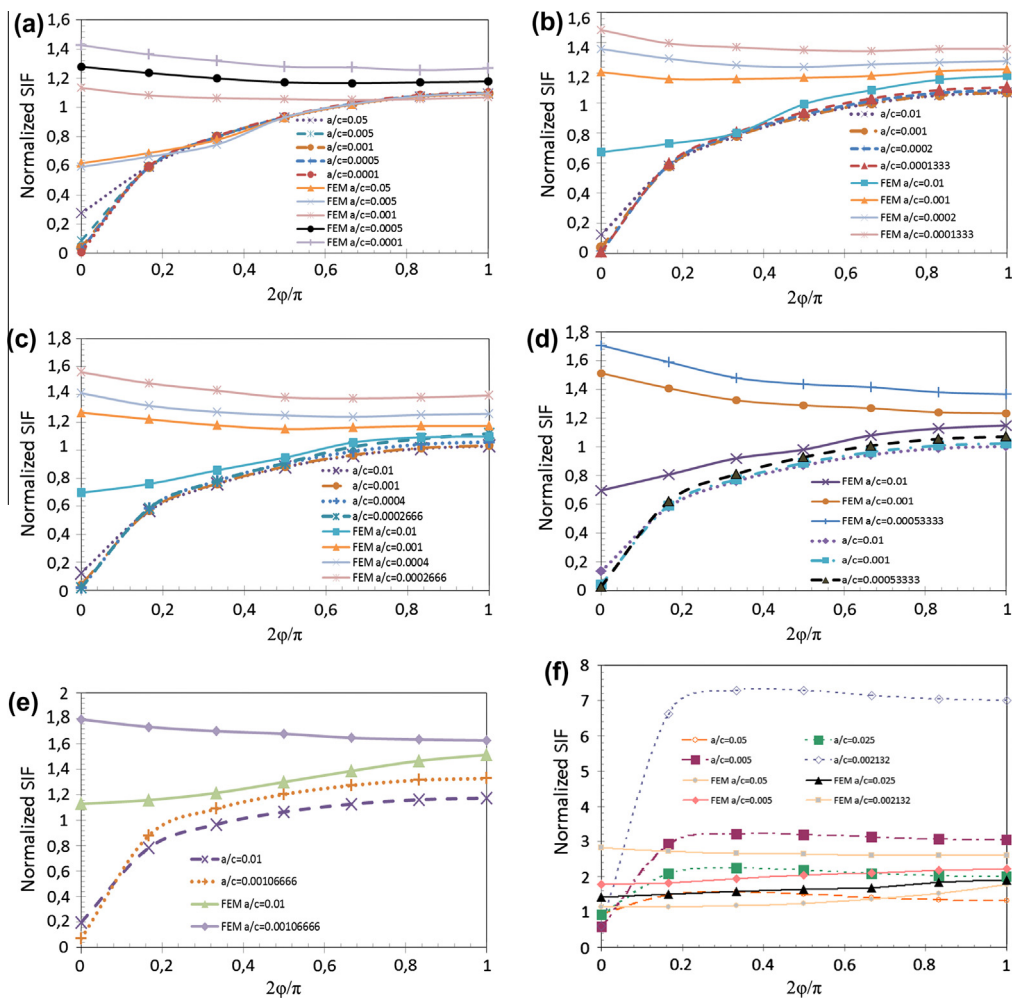


Fig. 10. Comparison of Normalized SIF between the FEM solutions and existing equations for cracks with depths, (a) 0.005 mm, (b) 0.01 mm, (c) 0.02 mm (d) 0.04 mm (e) 0.08 mm (f) 0.16 mm for long crack ($a/c \leq 0.025$).

Fig. 2 shows the built model from the realistic multi-crystalline silicon wafer used for a static 4-point bending test. The effect of anisotropy on the stress ratio (average stress distributed in anisotropic wafer divided over the average stress distributed in isotropic wafer) has been studied. An approximate 4% discrepancy is observed between different cases (50 different anisotropic cases) with different material orientation. Therefore, the isotropic silicon model works as well as the anisotropic multi-crystalline silicon wafer in terms of nominal stress.

The crack geometries analyzed in this study are listed in Table 1. The appropriate J -integral can be extracted from the very fine mesh around the crack tip (Fig. 3). 24,871 elements are used in this model. The element size and number were obtained after a mesh refinement study. 10 contour integrals were recognized as appropriate to determine $J(K_I)$. The preliminary studies showed that after 5th contour, the J -integral values converged. The differences between 8th and 10th contour integral were less than 0.4%, and the tenth contour value was employed. The finite element models for different crack geometries are built and solved using ABAQUS®/Standard. Although nonlinearities are considered, the simulation times for these models are reasonable (less than 1 h on a single W3670, 3.2 GHz processor machine).

4. Results and discussion

4.1. Effect of geometrical nonlinearity

In order to study the effect of the geometrical nonlinearity, two cases are considered, one accounting for large displacements, the other based on linear kinematics. Figs. 4–6 show the SIF versus the mid-point displacement for different crack geometries with both linear and nonlinear formulations. The horizontal line corresponds to the fracture toughness (K_{IC}) for the material. Significant difference is observed between linear and nonlinear formulations. It is interesting to note that

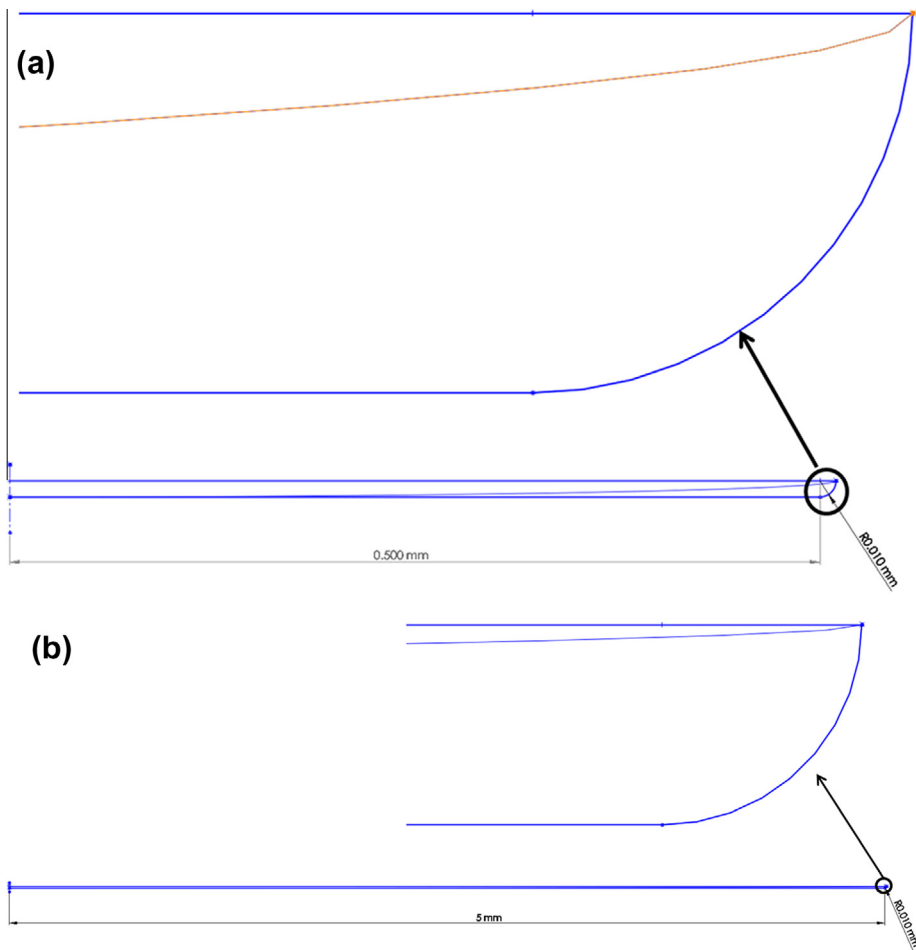


Fig. 11. Elliptic surface cracks with length (a) $2c = 1$ mm and (b) $2c = 10$ mm.

the difference between SIFs calculated by linear and nonlinear formulations depends on the surface crack size. The results indicate that SIF increases more in the nonlinear case compared to the linear one when the surface crack size increases. Considering the transverse displacement at brittle fracture, the discrepancy between linear and nonlinear models is 19% for a crack of $20\ \mu\text{m}$ depth and 1 mm length (see Figs. 4–6). This discrepancy increases to 74% for a crack of $160\ \mu\text{m}$ depth and 100 mm length. Therefore, accounting for geometrical nonlinearity is important in analysis of surface cracked ultra-thin silicon wafers. These results also correspond well to the findings in [19].

4.2. Comparison between semi-analytical equation and FEM results

In the following, SIFs from finite element analysis considering geometrical nonlinearity and the semi-analytical equation are presented for semi-elliptical surface cracked thin silicon wafers. It is important to note that although the Newman–Raju equation is valid for $c/W < 0.5$, larger ratios are also considered to investigate the validity for the cases $c/W \geq 0.5$.

The SIF for the crack geometries introduced in Table 1 is calculated by Newman–Raju equation. In addition, K_I from FEM was calculated for the same cases presented in Table 1. For cases in the range of $0.25 \leq a/c \leq 0.8$, the semi elliptic shape (model A) is used and model B is employed for the range of $0.0001 \leq a/c < 0.25$. Fig. 7 shows the stress distribution of model B for a crack of $20\ \mu\text{m}$ depth and 1 mm length.

A normalized SIF-ratio is employed, defined as the SIF divided by $\sigma_b \sqrt{\frac{\pi a}{Q}}$. Fig. 8 shows a good agreement of the normalized SIFs between Newman–Raju equation and FEM as functions of the parametric angle and a/c ratio for semi-elliptical surface cracks ($0.25 \leq a/c \leq 0.8$). For instance, approximately 12% discrepancy is obtained for the cracks with depths of 0.005 and 0.01 mm as shown in Fig. 9. Although Newman–Raju and FEM solutions display similar trends for short semi-elliptical surface cracks, they show significant discrepancy for long surface cracks. As shown in Fig. 10, the normalized SIFs diverge from each other at $\phi = 0$. The normalized SIF obtained from FEM using model B increases with the increase in crack length, while the SIF reduces with the crack length in the Newman–Raju equation. For instance, the normalized SIF is approximately 1.44 for a

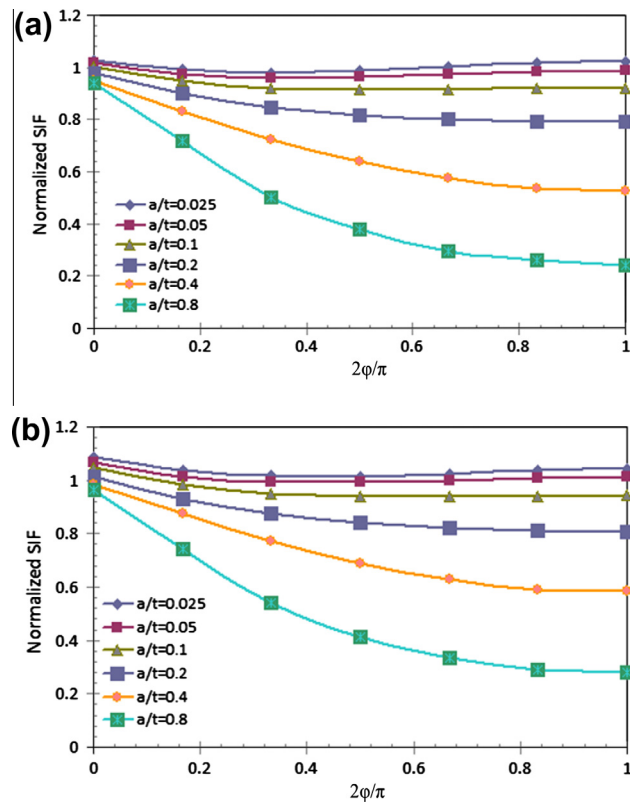


Fig. 12. Normalized SIF when $a/c = 0.8$ for (a) Newman–Raju equation and (b) FEM results.

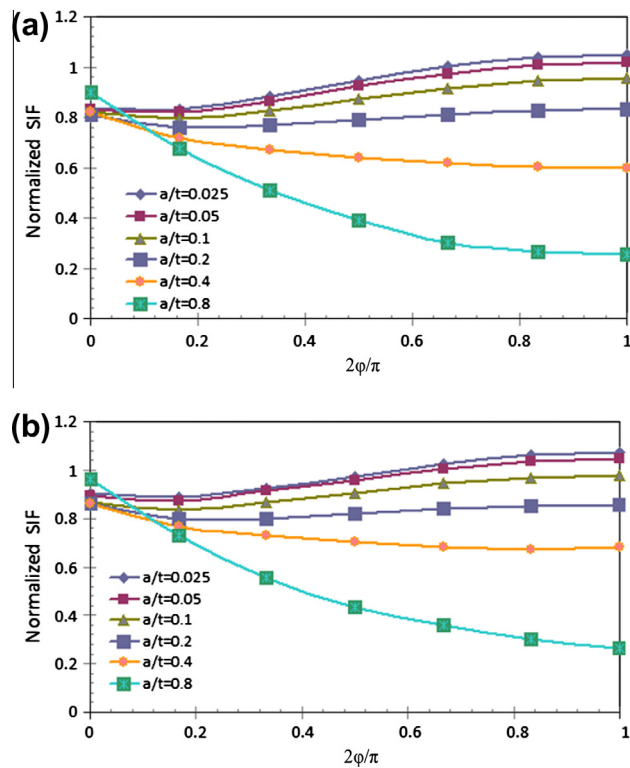


Fig. 13. Normalized SIF when $a/c = 0.5$ for (a) Newman–Raju equation and (b) FEM results.

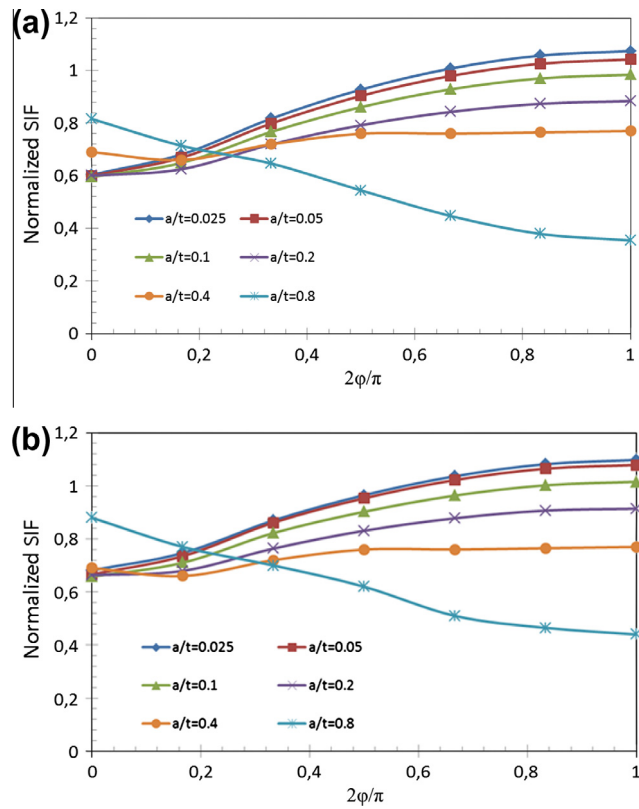


Fig. 14. Normalized SIF when $a/c = 0.25$ for (a) Newman–Raju equation and (b) FEM results.

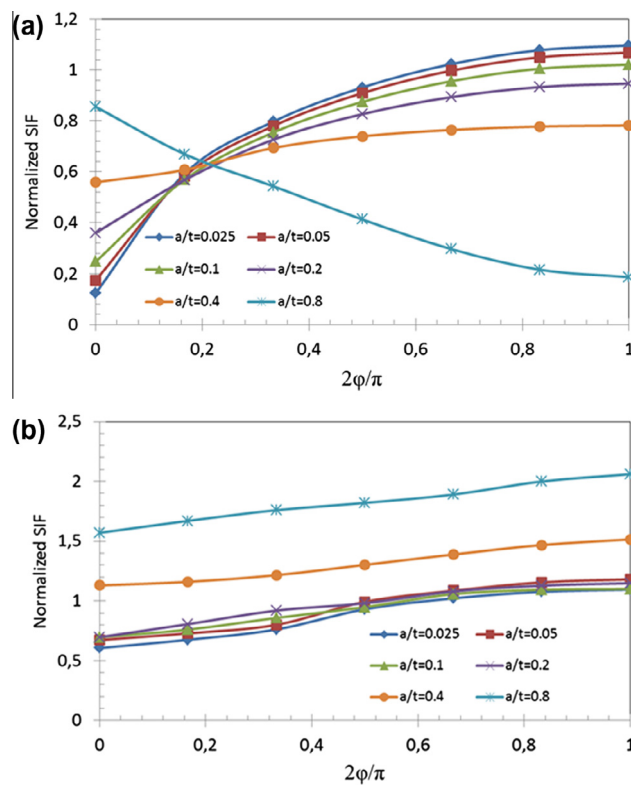


Fig. 15. Normalized SIF when $a/c = 0.01$ for (a) Newman–Raju equation and (b) FEM results.

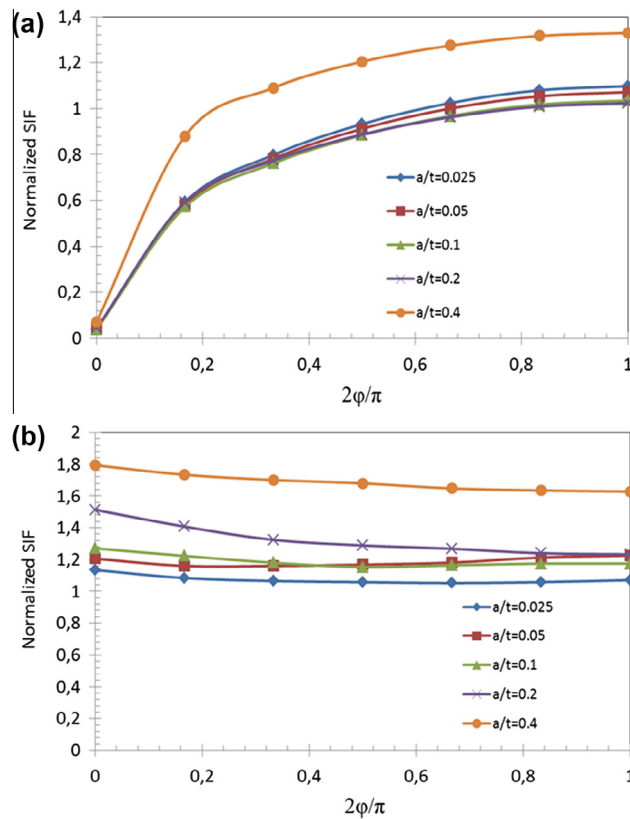


Fig. 16. Normalized SIF when $a/c = 0.001$ for (a) Newman–Raju equation and (b) FEM results.

crack with 50 mm length and 0.005 mm depth when model B is used and the normalized SIF for a similar crack shape is almost zero when the Newman–Raju equation is employed. The same trend is observed in Fig. 10 for other crack geometries at the front surface ($\phi = 0$). Stretching the length of semi-ellipse, the transition between the crack front and plate surface becomes smoother at $\phi = 0$. Therefore, reduction in normalized SIF is expected. This phenomenon becomes more critical for larger cracks. Two elliptic cracks with the same $a = 0.01$ mm and different length are illustrated in Fig. 11. The crack front curvature at the end regions for the semi elliptic crack is much smaller than the curvature in model B which is used in FEM. As shown in Fig. 10 for model B, the normalized SIF never becomes smaller than ≈ 0.6 at $\phi = 0$ and it increases with the reduction of a/c ratio. Model B is regarded as more conservative than Newman–Raju equation. It is also demonstrated in Fig. 10 that the maximum value of the normalized SIF occurs at $\phi = \pi/2$ for larger a/c ratios ($a/c \geq 0.001$). Comparing results with Newman–Raju, a higher normalized SIF is predicted with FEM for all ratios of a/c .

Figs. 12–16 display the variation of normalized SIF versus a/t for different values of a/c . The results given by the Newman–Raju solution are shown in Figs. 12(a)–16(a). It is observed from Fig. 12(a) that for $a/c = 0.8$ any point on the crack front (from $\phi = 0$ to $\pi/2$), the normalized SIF decreases with increasing of a/t , and this reduction will be larger when moving from the front surface ($\phi = 0$) where the maximum difference is 8% towards the crack center ($\phi = \pi/2$) where the difference is almost 80%. The reduction becomes larger for larger a/t (≥ 0.4). Although the same trend as Fig. 12(a) is shown in Figs. 13(a)–15(a) at the crack center ($\phi = \pi/2$), the reduction in the normalized SIF values is also observed at the front surface ($\phi = 0$). This reduction increases for long cracks (small ratios of a/c). As illustrated in Fig. 16(a) the normalized SIF is approximately zero for all a/t values at the front surface ($\phi = 0$). It means that the angle between the crack front and surface of wafer is very close to zero and therefore, the shape is very smooth and there is no significant stress concentration at $\phi = 0$. In fact, two opposite effects influence the SIF: curvature of the crack front at $\phi = 0$ (at intersection between crack and surface of wafer) and the ligament of the material in width direction, $F(c/w)$.

The curvature effect dominates over the ligament effect in width direction ($F(c/w)$) in the Newman–Raju equation for thin wafer. Compared to the Newman–Raju solution, the results from FEM (see Figs. 12(b)–16(b)) show both the effect of ligament and crack shape on the SIF. Figs. 12(b)–14(b) display the same trend as shown in Figs. 12(a)–14(a) for all curves. In contrast to Figs. 15(a) and 16(a) and 15(b) and 16(b) show that the normalized SIF increases when a/c decreases ($a/c \leq 0.01$). The maximum discrepancy can be observed in Fig. 16(b) where the ligament effect in width direction ($F(c/w)$) is the largest one ($2c \approx 150$ mm). The normalized SIF from the finite element analysis reaches to its maximum value at $\phi = 0$ for all ratios of a/t .

5. Conclusion

Stress intensity factors calculated with Newman–Raju solution and 3D finite element analysis for surface cracked silicon wafers subjected to bending were compared. The present study covers a wide range of configuration parameters. The ratio of crack depth to wafer thickness (a/t) varied from 0.025 to 0.8; the ratio of crack depth to crack length (a/c) changed from 0.001 to 0.8. The finite element analysis illustrated some limitations with the Newman–Raju approach in calculating SIFs for thin wafers. The limitations increase with the decrease of a/c . The results showed that the Newman–Raju solution predicts vanishing SIFs of the surface point ($\phi = 0$) for long surface cracks ($a/c \leq 0.01$). This indicates that finite element analysis is needed to predict the SIF for long surface cracks in ultra-thin silicon wafers. Also, due to the finite out of plane displacements in the wafer, geometrical nonlinearity should be included in the assessments.

Reference

- [1] Irwin GR. The crack extension force for a part-through crack in a plate. *ASME J Appl Mech* 1962;29:651–4.
- [2] Green AE, Sneddon IN. The distribution of stress in the neighborhood of a flat elliptical crack in an elastic solid. *Proc Cambridge Phil Soc* 1950;47:159–64.
- [3] Kassir MK, Sih GC. Three-dimensional stress distribution around an elliptical crack under arbitrary loadings. *J Appl Mech* 1966;88:601–11.
- [4] Shah RC, Kobayashi AS. Stress-intensity factor for an elliptical crack under arbitrary normal loading. *Engng Fract Mech* 1971;3:71–96.
- [5] Vijayakumar Ko, Atluri SN. An embedded elliptical flow in an infinite solid, subject to arbitrary crack-face tractions. *J Appl Mech* 1981;48:88–96.
- [6] Smith FW, Emery AF, Kobayashi AS. Stress intensity factors for semi-circular cracks, Part 2 – Semi-infinite solid. *J Appl Mech Trans ASME* 1967;89:953–9.
- [7] Kobayashi AS. Crack-opening displacement in a surface flawed plate subjected to tension or plate bending. In: *Proc. second int. j. conf. on mechanical behavior of materials*, ASM; 1976. p. 1073–7.
- [8] Raju IS, Newman JC. Stress-intensity factors for a wide range of semi elliptical surface cracks in finite-thickness plates. *Engng Fract Mech J* 1979;11:817–29.
- [9] Newman JC, Raju IS. Analyses of surface cracks in finite plates under tension or bending loads. NASA TP-1578; 1979.
- [10] Nishioka T, Atluri SN. Analytical solution for embedded elliptical cracks, and finite element-alternating method for elliptical surface cracks, subjected to arbitrary loadings. *Engng Fract Mech* 1983;17:247–68.
- [11] Heliot J, Labbens R, Pellissier-Tanon A. Benchmark problem no. i – semi elliptical surface crack. *Int J Fract* 1979;15:R197–202.
- [12] Pickard A. Stress intensity factors for cracks with circular and elliptic crack fronts-determined by 3D finite element methods. PNR-90035, Rolls-Royce Limited; 1980.
- [13] Funke C, Kollig E, Kuna M, Möller J. Biaxial fracture test of silicon wafers. *Adv Engng Mater* 2004;6:596–8.
- [14] Pandolfi Weinberg. A numerical approach to the analysis of failure modes in anisotropic plates. *Engng Fract Mech* 2011;78:2052–69.
- [15] Yoon J, Chaudhuri RA. Three-dimensional singular antiplane shear stress fields at the fronts of interfacial crack/anticrack/contact type discontinuities in tricrystal anisotropic plates. *Engng Fract Mech* 2013;102:15–31.
- [16] Birringer RP, Chidester PJ, Dauskardt RH. High yield four-point bend thin film adhesion testing techniques. *Engng Fract Mech* 2011;78:2390–8.
- [17] Wortman JJ, Evans RA. Young's modulus, shear modulus, and poisson's ratio in silicon and Germanium. *J Appl Phys* 1965;36:153–6.
- [18] Ravi KV. The growth of EFG silicon ribbons. *J Cryst Growth* 1977;39:1–16.
- [19] Saffar S, Gouttebroze S, Zhang ZL. Fracture analysis and distribution of surface cracks in multi crystalline silicon wafers. *J Sol Energy Engng* 2013;136(2):021024 (1–9).